Anomalous gelation of self-assembling ethanol molecules

Takaaki Sakai[1,2,3]*, Ryoichi Kanega[3], Akihiro Ohira[1,3], Eiji Hosono[1,3,4], Daisuke Asakura[1,3,4], Takuya Yamaguchi[3], Tomohiro Ishiyama[1,3], Katherine Develos-Bagarinao[1,3], Koji Ohara[5], Toshiaki Ina[5], Haruo Kishimoto[1,3] & Masatsugu Oishi[6]

[1] Global Zero Emission Research Center, National Institute of Advanced Industrial Science and Technology (AIST), 16-1 Onogawa, Tsukuba, Ibaraki 305-8569, Japan
[2] Center for Molecular Systems (CMS), Kyushu University, 744 Motooka, Nishi-ku, Fukuoka 819-0395, Japan
[3] Research Institute of Energy Conservation, National Institute of Advanced Industrial Science and Technology (AIST), 1-1-1 Higashi, Tsukuba, Ibaraki 305-8565, Japan
[4] AIST-UTokyo Advanced Operando-Measurement Open Innovation Laboratory (OPERANDO-OIL), National Institute of Advanced Industrial Science and Technology (AIST), Kashiwa, Chiba 277-8565, Japan
[5] Japan Synchrotron Radiation Research Institute (JASRI), 1-1-1 Kouto, Sayo-cho, Sayo-gun, Hyogo 679-5198, Japan
[6] Graduate School of Technology, Industrial and Social Science, Tokushima University, 2-1 Minamijosanjima cho, Tokushima 770-8506, Japan

* Corresponding author. Email: sakai-takaaki@aist.go.jp

Abstract

A low-molecular-weight gel is one that is organized by small molecules via noncovalent bonds[1-5], and some low-molecular-weight gels already being used in our daily lives[6]. In general, the mechanism of formation of low-molecular-weight gels involves the gelation of solvents such as ethanol and water in the presence of low-molecular-weight gelators, which have larger molecular weights than the solvents. The gelator creates a supramolecular network via noncovalent bonds[7], and this network holds the solvent molecules, causing them to lose fluidity and thereby promoting gelation. That is, low-molecular-weight gels do not self-assemble and gelate solvent molecules themselves; the literature contains no reports of the self-assembly and gelation of extremely small solvent molecules such as ethanol and water. However, in this work, we found that ethanol molecules themselves form a large gel structure by self-assembling with few-nanometer-diameter oxide nanoparticles and water molecules. Our finding reveals an intriguing phenomenon where ethanol molecules support the main structure of a large gel structure through supramolecular assembly via hydrogen bonding. The key factor for the gelation of ethanol observed in this study is the presence of $BaZrO_3$ nanoparticles, which are positively charged and homogeneously dispersed. When these nanoparticles and water were present, we observed the gelation of a substantial amount of ethanol, which would not normally occur. Our results overturn the common belief that extremely small molecules such as ethanol cannot function as a main bearer of gelatinization, and our discovery opens a path to the development of

a novel self-assembly system that has not been previously reported. In addition, because the method proposed in the present work can potentially be used to prepare gels that incorporate other extremely small molecules having hydrogen bonds, we expect our findings to lead to the development of various novel materials with unique functions.

Main Text

A low-molecular-weight gel is one that is organized by small molecules via noncovalent bonds such as hydrogen bonds or by van der Waals forces. Because noncovalent bonds exhibit reversibility, the structure of low-molecular-weight gels can be changed by recombining these bonds under external stimuli, enabling the properties and functions of the gel to be arbitrarily controlled[1]. This feature is a great advantage not found in polymers. Various low-molecular-weight gels, such as organogels and hydrogels, are being intensively researched and developed[1-5], and some of them are already used in our daily lives. For example, classically, 1,2-hydroxystearic acid is widely used as a gelator for waste oil treatment in households[6].

In general, such gels are formed by adding a low-molecular-weight gelator to a solvent, where the gelator has a larger molecular weight than the solvent, causing the solvent to lose fluidity by being retained in a supramolecular assembly network as a result of noncovalent bonding of the gelator. Thus far, gelation of low-weight-molecular gels by hydrogen bonding of the solvent itself (e.g., ethanol or water, both of which have extremely low molecular weights) has not been reported. In the case of ethanol, although the literature contains several accounts of interactions such as OH linkages of ethanol on a silica surface in cyclohexane solution[8-9], clustering of ethanol in ethanol–water mixtures[10], and short-range ordering of ethanol on zinc oxide nanoparticles[11], extensive gel formation by hydrogen bonding with ethanol itself on a visible level has not been reported. However, as a method to gelate ethanol, dissolution and precipitation of calcium acetate in ethanol are commonly used[12]. However, this method also simply retains the ethanol molecules between the precipitated calcium acetate fibers rather than inducing gelation of the ethanol molecules themselves via multiple hydrogen bonds. A similar example is the use of perfluoroalkyl-chain-containing organogelators, which create low-molecular-weight fibers that hold and gelate ethanol[7]. As such, the common belief at present is that ethanol never functions as the main bearer of a gel structure but instead functions as a solvent that is retained between the structures by the gelator. However, in the present work, we found that ethanol itself can form large gel structures via hydrogen bonds with oxide nanoparticles a few nanometers in diameter and water molecules. The resultant gel can also be considered an inorganic/organic hybrid gel (i.e., an inorganic/organic hybrid molecular system). In the case of inorganic/organic systems, Shinkai et al. have reported hybrid gels of nanofullerenes and tetraphenylporphyrin (1b) bearing amide groups at the 3,5-positions of the meso-phenyl groups[13]; however, our finding of a hybrid molecular system is also interesting because the molecular size of the main bearer of the gelation is much smaller than any previously used molecules.

The appearance of gelated ethanol is shown in Fig. 1a,b. In this case, the sample was obtained by adding $BaZrO_3$ (BZO) powder to ethanol and milling the mixture with very small zirconia

beads in a high-speed planetary mill (see Extended Data Figs. 1 and 2)[14-19]. When 0.05 mm-diameter (50 μm) zirconia beads were used, a finely dispersed BZO nanoparticle–ethanol slurry with a most common particle size on the order of several nanometers was obtained[14,18]. In fact, as shown in Fig. 2a,b, the most common particle size was ~2 nm and the particles exhibited a positive zeta potential of ~50 mV (+50 mV). After bead milling, the slurry was in liquid form (Extended Data Fig. 2); however, the slurry solidified as it absorbed moisture in the air and gelated to the extent that it could be scooped with a spoon (Fig. 1). In addition, the slurry gelated easily when water was intentionally added (Extended Data Fig. 3a).

We first consider the assumption that the positively charged nanoparticles, ethanol, and a small amount of water formed hydrogen bonds in the structure shown in Fig. 1c,d when water was added to the slurry. Even when a small amount (50 μL) of water was added to a slurry volume of 1 mL (0.5 vol% H_2O addition to 100 vol% slurry), gelation was eventually confirmed (Extended Data Fig. 3a). However, as shown in the Karl Fischer titration results (Extended Data Fig. 4 and Extended Data Table 1), 0.6 to 1.0 wt% of water was already contained in the slurry after bead milling. For example, the slurry used in Extended Data Fig. 3a contained 0.77 wt% water and the addition of 0.5 vol% water to the slurry of 100 vol% resulted in a total water content of ~1.3 wt%. That is, the slurry after bead milling already contained an almost gelatinous amount of water, and the addition of even a small amount of water was sufficient to cause gelation. This explanation is also applicable to the phenomenon of spontaneous gelation of the slurry (Fig. 1). In addition, the degree of gelation when the amount of nanoparticles was reduced is shown in Extended Data Fig. 3b. The results show that gelation occurred even when the amount of nanoparticles was reduced to approximately 2 wt%. Because the density of BZO is ~6.11 g/cm^3, when water was added to the slurry at a ratio of 3:100 vol%, the volume ratio of BZO nanoparticles in the gel was ~0.7 vol% (see the calculation in Methods) in the case of 5 wt% BZO nanoparticles[20]. When the amount of BZO nanoparticles was 2 wt%, its volume ratio was ~0.3 vol%; that is, even though the volume ratio of ethanol (+ a small amount of H_2O) was ~99.7 vol%, the gel still eventually formed.

As another possible explanation for gelation other than hydrogen-bond formation, we cannot exclude the possibility that the BZO nanoparticles were decomposed by the addition of H_2O and that a chain-like material such as zirconium-derived polymetalloxane[21], which might induce gelation, was formed. Therefore, X-ray absorption fine structure (XAFS) (i.e., X-ray near edge fine structure (XANES) and extended X-ray absorption fine structure (EXAFS)) measurements were carried out to investigate the possibility that the nanoparticles decomposed or that major changes occurred in their crystal structure after gelation. From the Zr K-edge XANES and EXAFS spectra in Fig. 3a,b, the Zr^{4+} state in a perovskite-type structure was confirmed in both cases[22,23] and almost no changes were observed in the XANES spectra and EXAFS oscillations, suggesting that the electronic and local structures of BZO before and after gelation were similar (Fig. 3c). Similarly, from a pair distribution function (PDF) analysis (Fig. 3d and Extended Data Fig. 5), no difference was observed before and after gelation. These results indicate that the perovskite structure of the BZO nanoparticles was maintained after the addition of H_2O. The

XRD patterns for the bead-mill slurry and gel (Extended Data Fig. 6) also show that the perovskite structure of the nanoparticles was maintained after gelation[24]. Moreover, thermodynamic calculations (Extended Data Fig. 7) show that BZO does not decompose upon addition of H_2O, unlike Ba carbonated with CO_2[25]. Thus, on the basis of the present experimental evidence, we can eliminate the possibility that the BZO decomposed into gelation-inducing materials as a result of the addition of H_2O.

We also cannot disregard the possibility that the nanoparticles formed a fiber-like material upon the addition of water, leading to the formation of a three-dimensional structure and the gelation of ethanol. To examine this possibility, we first froze the gel using liquid N_2 and then freeze-dried it to determine whether we could obtain a xerogel (Extended Data Fig. 8a); however, we could not confirm the formation of a xerogel-like material. The freezing of the gel was insufficient because the freeze-drying temperature was approximately −50 °C and the freezing point (fp) of ethanol is −114 °C. We replaced the ethanol of the nanoslurry with dimethylsulfoxide (DMSO, fp 19 °C) and induced gelation by adding H_2O. The DMSO-replaced gel was also freeze-dried to check whether a xerogel could be obtained (Extended Data Fig. 8b). Similarly, we could not confirm the formation of a xerogel-like material. Therefore, we can exclude the possibility that the gelation was caused by a fiber-like material formed via the aggregation of nanoparticles.

Another possibility is that the addition of H_2O changed the ethanol into a polymer-like material. In the ^{1}H-NMR spectra of ethanol before and after gelation (Extended Data Fig. 9), only the signal for ethanol was observed in both cases (Extended Data Fig. 9). In addition, spectral features associated with ethanol were observed in FT-IR spectra acquired before and after gelation (Supplemental Figure 2)[26]. Furthermore, the results of low-temperature differential scanning calorimetry (DSC) measurements (Extended Data Fig. 10 and Extended Data Table 2) show that the crystallization and melting points of the slurry and gel agree well with those of ethanol mixed with the same amount of water. These results thus indicate that ethanol is not changed into a polymer-like organic material and that ethanol itself is not changed by the addition of H_2O. Hence, the gelation occurs through hydrogen bonding with ethanol. In fact, a change in the OH peak for ethanol was observed in the ^{1}H-NMR spectra acquired after gelation. Fig. 2c shows a magnified figure of the OH peak in the ^{1}H-NMR spectra. The OH-derived signal after gelation distinctly differs from that in the spectra of the other samples, and it is shifted to higher magnetic field. The chemical shift of the proton signal has been reported to be correlated with the hydrogen-bond length[27,28], and the shift to a higher magnetic field indicates that the hydrogen-bond length for ethanol is increased after gelation.

On the basis of the previously discussed results, we here propose a mechanism for gelation of a BZO nanoparticle slurry upon H_2O addition (Fig. 4). The average distance between the nanoparticles is ~8.6 nm, whereas the kinetic diameter of ethanol is ~0.45 nm[29]. Hence, there are ~20 ethanol molecules between the nanoparticles. The BZO nanoparticles are positively charged

even before gelation. Therefore, some of the ethanol (and H_2O included in the slurry from the beginning) are strongly bound to the BZO nanoparticles, forming hydrogen-bonded clusters to some extent, and the other ethanol and H_2O molecules also individually form small clusters[10]. The hydrogen-bonding network will be interrupted in the middle, and no gelation will be observed. However, if a small amount of H_2O molecules having many hydrogen-bonding points are added to the slurry, and the molecules occupy appropriate locations, an overall hydrogen-bonding network forms and the slurry undergoes gelation. In this case, the hydrogen bonding length increases slightly because the ethanol molecules need to be uniformly distributed, which is a possible reason for the aforementioned high-magnetic-field shift observed in the ^{1}H-NMR spectra. That is, gelation of the slurry was caused by a slight increase in hydrogen bonding as a result of H_2O addition and by a slight change in the hydrogen-bonding length for ethanol. In the corresponding FT-IR attenuated total reflection (ATR) spectra (Extended Data Fig. 11), the peak due to OH stretching vibration did not substantially change after gelation. It is reasonable to assume that, even though the amount of hydrogen bonds is increased slightly after gelation, the length of hydrogen bonds is also increased and the strength of each bond is decreased slightly, resulting in offsetting effects in the ATR spectrum. As a result, changes that would be difficult to observe become even more difficult to detect; thus, no substantial changes were evident in the ATR spectrum. In summary, the key factor in the gelation of ethanol observed in the present study is the presence of BZO nanoparticles, which are positively charged and homogeneously dispersed. When these nanoparticles and H_2O were present, gelation of a substantial amount of ethanol occurred. Because the nanoparticles prepared in this work might be applicable to induce gelation of other low-molecular-weight molecules having hydrogen bonds, our method has the potential to create various functional gels incorporating a wide range of small molecules.
(1956 words)

Methods
Synthesis

BZO powder was synthesized by mixing $BaCO_3$ and ZrO_2 powders with ethanol in a mortar and calcining the resultant mixture at 1200 °C for 10 h in air. Yttria-stabilized zirconia (YSZ) milling beads and pots were used with a planetary ball-milling machine (Fritsch Pulverizette 7, FRITSCH) for bead milling. The nanoparticle slurry was prepared using the following procedure: BZO powder was first pulverized at 500 rpm for 1 h with ⌀2 mm balls in ethanol, and the ⌀2 mm balls were subsequently separated using a sieve. YSZ beads with a diameter of ⌀0.05 mm were then added to the slurry, and milling was performed at 800 rpm for a total of 7 h. Details of the bead-milling procedure are shown in Extended Data Fig. 1. After the bead-milling process, the obtained nanoparticle slurry was centrifuged to remove coarse particles (except the slurry shown in Extended Data Fig. 2). The concentration of BZO in the slurry used in this work was kept constant at ~5 wt% unless otherwise noted. The bead milling was performed at approximately room temperature. *Note: If the ambient temperature during milling is too low, pulverization to fine nanoparticles may not proceed properly.

Dynamic light scattering and zeta-potential measurements

Particle size and zeta-potential measurements were carried out using a dynamic light scattering (DLS)–zeta-potential measurement system (Zetasizer Pro, Malvern Panalytical). In addition, the particle size and zeta potential were calculated using the dielectric constant and viscosity of ethanol. *Note: the DLS system cannot properly observe small particles in the presence of coarse particles because the intensity of the reflected light from the particles depends on the sixth power of the particle size ($\propto r^6$), as per the measurement principle of the DLS system; the coarse particles were therefore removed by centrifugation.

^{1}H nuclear magnetic resonance (NMR) spectra

^{1}H NMR spectra were recorded at 25 °C on a 60 MHz NMR spectrometer (X-Pulse, Oxford Instruments), and spectra were referenced to tetramethylsilane (TMS) as an internal standard. To ensure that the TMS was not contaminated by the samples, the TMS was placed in quartz glass sample tubes (⌀2.0 mm). The scan data were collected using the soft-lock mode: after the first scan, the largest peak in the spectrum was found and the peak was set as the soft-lock peak. All subsequent scans were aligned to the soft-lock peak.

X-ray absorption fine structure (XAFS) (X-ray absorption near edge structure, XANES, extended X-ray absorption fine structure, EXAFS)

XAFS (XANES and EXAFS) measurements at the Zr *K*-edge were performed using beamline BL01B1 at SPring-8 (Hyogo, Japan)[30]. The Zr *K*-edge spectra were recorded in transmission mode using a Si(311) double-crystal monochromator. The energy scale was calibrated using a Zr foil. The intensities of the incident and transmitted X-rays were simultaneously monitored by ionization chambers. The XAFS spectra were analyzed using the IFEFFIT program code in ATHENA[31].

Pair distribution function analysis

High-energy X-ray total scattering experiments were carried out at SPring-8 beamline BL04B2 using a two-axis diffractometer[32,33]. The incident X-ray energy obtained via a Si(220) crystal monochromator was 61.4 keV. The samples were sealed in capillary tubes. The measurements were performed in transmission geometry with a 2θ angle from 0.3° to 49°, corresponding to a Q-range from 0.2 to 25 Å^{-1}. The PDF profiles were obtained using the in-house BL04B2 software. The X-ray total structure factor, $S(Q)$, was derived from the scattering intensity. The reduced PDF, $G(r)$, was obtained by the Fourier transformation of $S(Q)$:

$$G(\mathrm{r}) = \frac{2}{\pi} \int_{Q_{\min}}^{Q_{\max}} Q\{\mathrm{S}(Q) - 1\}\sin(Q\mathrm{r})\mathrm{d}Q,$$

where $Q_{\max}$ and $Q_{\min}$ are the maximum and minimum observed Q values, respectively.

Powder X-ray diffraction

Powder XRD measurements were carried out by scanning the samples from 10° to 90° using a benchtop powder X-ray diffractometer (D2-Phaser, Bruker AXS). As shown in the thermodynamic calculation in Extended Data Fig. 6, BZO easily reacts even with the 410 ppm

CO_2 contained in ambient air near room temperature. Thus, the bead-mill slurry was dried under vacuum and the measurements were performed immediately. In the case of ethanol, the measurement was performed by placing liquid ethanol directly in a normal dish-type sample holder.

Karl Fischer titration

The H_2O content in slurries and ethanol was evaluated by Karl Fischer titration using an MKC-710 (Kyoto Electronics Manufacturing).

Thermodynamic calculations

Thermodynamic calculations for BZO against H_2O and CO_2 were carried out using MALT-2 (Kagaku Gijutsu-sha).

Fourier transform infrared (FT-IR) spectroscopy (transmission method and attenuated total reflection (ATR) method)

For both the transmission method and the ATR method, the measurements were performed using an FT-IR spectrometer (FT-IR-4300, JASCO). For the transmission method, a commercially available liquid cell equipped with CaF_2 windows was used. A diamond window-type measurement kit (ATR-Pro One, JASCO) was used for the ATR measurements.

Low-temperature differential scanning calorimetry (DSC)

DSC measurements were performed using a differential scanning calorimeter (DSC 2920, TA Instruments). The samples were mounted in an Al-type sample holder and were cooled by liquid N_2 for 5 min; the measurements were then performed as the temperature was increased at 10 °C/min.

Calculation of volume ratio and distance between particles

*5 wt% BZO nanoslurry + 100:3 vol% H_2O addition.

-Volume ratio

BZO: 1 g, ethanol: 19 g

(Note: To simplify the calculations, the effects of small amounts of water (~1 wt%) already present in the slurry were ignored; the volume ratio does not substantially change if we assume the initial water content.)

BZO density: 6.11 g/cm^3, ethanol: 0.789 g/cm^3

Volume of BZO: $1/6.11 = 0.164$ cm^3, ethanol: $19/0.789 = 24.081$ cm^3 in the slurry.

Thus, the BZO volume ratio in the nanoslurry is $0.164/(24.081 + 0.164) \times 100 = 0.68\%$.

For the gel, BZO nanoslurry: $H_2O = 100: 3$ vol; thus, the BZO volume fraction in the gel is $0.68/100/103 = 0.66 \cong 0.7\%$.

-Distance between particles

If we assume that BZO is composed of 2 nm spherical particles (radius: 1 nm),

BZO particle volume: $4/3 \times 3.1415 \times 1 = 4.19$ nm^3, where the volume ratio of BZO particle and overall gel is 0.66:100. The overall slurry volume is 634.8 nm^3. Thus, the radius of the overall slurry is $(634.8/(4/3 \times 3.1415))^{1/3} = 5.33$ nm.

As shown in Fig. 1(c), the distance between particles is $5.33 \times 2 - 2 \cong 8.6$ nm.

*2 wt% slurry 100:3 vol% H$_2$O addition
-Volume ratio
BZO: 0.4 g, ethanol: 19.6 g
(Note: To simplify the calculations, the effects of small amounts of water already included in the slurry were also ignored.)
BZO density: 6.11 g/cm^3, ethanol : 0.789 g/cm^3.
Volume of BZO: $0.4/6.11 = 0.065$ cm^3, ethanol: $19.6/0.789 = 24.842$ cm^3.
Thus, the BZO volume ratio in the gel is $0.065/(24.842 + 0.065) \times 100/1.03 = 0.25 \cong 0.3\%$.

References
1. Sugiyasu, K., Fujita, N. & Shinkai, S. Design of novel composite materials by functional low molecular-weight organogels. *J. Synth. Org. Chem. Jpn* **63**, 359-369 (2005).
2. Terech, P. & Weiss, R. G. Low molecular mass gelators of organic liquids and the properties of their gels. *Chem. Rev.* **97**, 3133-3159 (1997).
3. Esch, J. H. & Feringa, B. L. New functional materials based on self-assembling organogels: from serendipity towards design. *Angew. Chem., Int., Ed.* **39**, 2263-2266 (2000).
4. Estroff, L. A. & Hamilton, A. D. Water gelation by small organic molecules. *Chem. Rev.* **104**, 1201-1208 (2004).
5 Wang, Q. et al. High-water-content mouldable hydrogels by mixing clay and a dendritic molecular binder. *Nature* **463**, 339-343 (2010).
6. Tachibana, T., Mori, T. & Hori, K. Chiral mesophases of 12-hydroxyoctadecanoic acid in jelly and in the solid state. i. a new type of lyotropic mesophase in jelly with organic solvents. *Bull Chem Soc Jpn*. **53**, 1714-1719 (1980).
7. Yamanaka, M., Sada, K., Miyata, M., Hanabusa, K. & Nakano, K. Construction of superhydrophobic surfaces by fibrous aggregation of perfluoroalkyl chain-containing organogelators. *Chem. Commun*. 2248-2250 (2006).
8. Mizukami, M., Moteki, M. & Kurihara, K. Hydrogen-bonded macrocluster formation of ethanol on silica surfaces in cyclohexane. *J. Am. Chem. Soc*. **124**, 12889-12897 (2002).
9. Andoh, Y., Kurahashi, K., Sakuma, H., Yasuoka, K. Kurihara, & K. Anisotropic molecular clustering in liquid ethanol induced by a charged fully hydroxylated silicon dioxide (SiO$_2$) surface. *Chem. Phys. Lett*. **448**, 253-257 (2007).
10. Wakisaka, A. Physicochemical properties of aqueous solutions from the viewpoint of cluster structures analyzed by mass spectrometry. *Bunseki Kagaku* **59**, 743-758 (2010).
11. Zobel, M., Neder, R. B. & Kimber, S. A. J. Universal solvent restructuring induced by colloidal nanoparticles. *Science* **347**, 292-294 (2015).
12. Henstrock, H. Calcium acetate gels. *Trans. Faraday Soc*. **29**, 1101-1107 (1933).

13. Shirakawa, M., Fujita, N. & Shinkai, S. [60]Fullerene-motivated organogel formation in a porphyrin derivative bearing programmed hydrogen-bonding sites. *J. Am. Chem. Soc.* **125**, 9902-9903 (2003).

14. Sakai, T., Hyodo, J., Ishihara, T. & Matsumoto, H. Single Nanosize Pulverization of solid oxide by means of a wet planetary-beads-milling. *J. Ceram. Soc. Jpn.* **120**, 39-42 (2012).

15. Sakai, T. et al. High Sinterabillity of Planetary-Bead-Milled Barium Zirconate, *Electrochemistry* **77** 876-878 (2009).

16. Oda, H., Yoneda, T., Sakai, T., Okuyama, Y. & Matsumoto, H. Preparation of nano-structured cathode for protonic ceramic fuel cell by bead-milling method. *Solid State Ionics* **262** 388-391 (2014).

17. Oda, H., Okuyama, Y., Sakai, T. & Matsumoto, H. Preparation of nano-structured $La_{0.6}Sr_{0.4}Co_{0.2}Fe_{0.8}O_{3-\delta}$ cathode for protonic ceramic fuel cell by bead-milling method. *Mater. Trans.* **55** 722-727 (2014).

18. Sakai, T., Okuyama, Y., Ishihara, T. & Matsumoto, H. Preparation and characteristics of proton conducting oxide nano-particles using planetary bead-mill. *2012 ECS Meet. Abstr.* **MA2012-02** 265 (2012).

19. Nakamura, M., Sakai, T., Kato, T., Koura, S. & Ohira, A. Fabrication of SOFC using $BaZr_{0.8}Y_{0.2}O_{3-\delta}$ nano-slurry electrolyte. *ECS Trans.* **91** 1053-1058 (2019).

20. Levin, I. et al. Phase equilibria, crystal structures, and dielectric anomaly in the $BaZrO_3$-$CaZrO_3$ system. *J. Solid State Chem.* **175** 170-181 (2003).

21. Gunji, T. et al. Preparation of polyzirconoxane from zirconium oxychloride octahydrate and ethylene glycol as a precursor for zirconia ceramics. *Appl. Organometal. Chem.* **14** 119-126 (2000).

22. Haskel, D., Ravel, B., Newville, M. & Stern, E. A. Single and multiple scattering XAFS in $BaZrO_3$: A comparison between theory and experiment. *Physica B: Condensed Matter* **208&209** 151-153 (1995).

23. Oishi, M. Et al. Evaluation of the electronic and local structure of mn in proton-conducting oxide, $Ca(Zr,Mn)O_{3-\delta}$, to elucidate a direct hydrogen-dissolution reaction. *J. Phys. Chem. C* **123**, 16034-16045 (2019).

24. Kennedy, B. J., Howard, C. J., Thorogood, G. J. & Hester, J. R. The influence of composition and temperature on the phases in $Sr_{1-x}Ba_xZrO_3$ perovskites: A high-resolution powder diffraction study. *J. Solid State Chem.* **161**, 106-112 (2001).

25. Matsumoto, H. et al. Hydrogen separation from syngas using high-temperature proton conductors. *Ionics* **13**, 93-99 (2007).

26. Doroshenko, I., Pogorelov, V. & Sablinskas, V. Infrared absorption spectra of monohydric alcohols. *Dataset Papers in Science* **2013**, Article ID 329406, 6 pages, (2013).

27. Sternberg, U. & Brunner, E. The influence of short-range geometry on the chemical shift of protons in hydrogen bond. *J. Magn. Reson. Series A* **108**, 142-150 (1994).

28 Lomas, J. S. ^{1}H NMR spectra of alcohols in hydrogen bonding solvents: DFT/GIAO calculations of chemical shifts. *Magn. Reson. Chem.* **54**, 28-38 (2016).

29. Wu, H., Gong, Q., Olson, D. H. & Li, J. Commensurate Adsorption of Hydrocarbons and

Alcohols in Microporous Metal Organic Frameworks. *Chem. Rev.* **112**, 836-868 (2012).

30. Uruga, T. et al. The XAFS beamline BL01B1 at SPring-8. *J. Synchrotron Rad.*, **6**, 143-145 (1999).

31. Ravel, B. & Newville, M. ATHENA, ARTEMIS, HEPHAESTUS: Data Analysis for X-Ray Absorption Spectroscopy Using IFEFFIT, *J. Synchrotron Radiat* **12**, 537-541 (2005).

32. Ohara, S. et al. Accurate synchrotron hard X-ray diffraction measurement on high-temperature liquid oxides, *Int. J. Microgravity Sci. Appl.* **37(2)**, 370202 (2020).

33. Kohara, S. et al. Structure of disordered materials studied by high-energy X-ray diffraction technique. Mater. Sci. Forum 706-709, 1690-1695 (2012).

Author contributions

Conceptualization: T.S.

Methodology: T.S., R.K., A.O., M.O.

Investigation: T.S., R.K., A.O., A.D., E.H., T.Y., T.I., T.I., K.O., M.O.

Visualization: T.S., R.K., A.O., M.O.

Project administration: T.S., H.K.

Writing- original draft: T.S., R.K., A.O., M.O.

Writing - review & editing: T.S., K.D.B., M.O.

All authors contributed to the final draft

Competing interests

The authors declare that they have no competing interests.

**Data and materials availability**

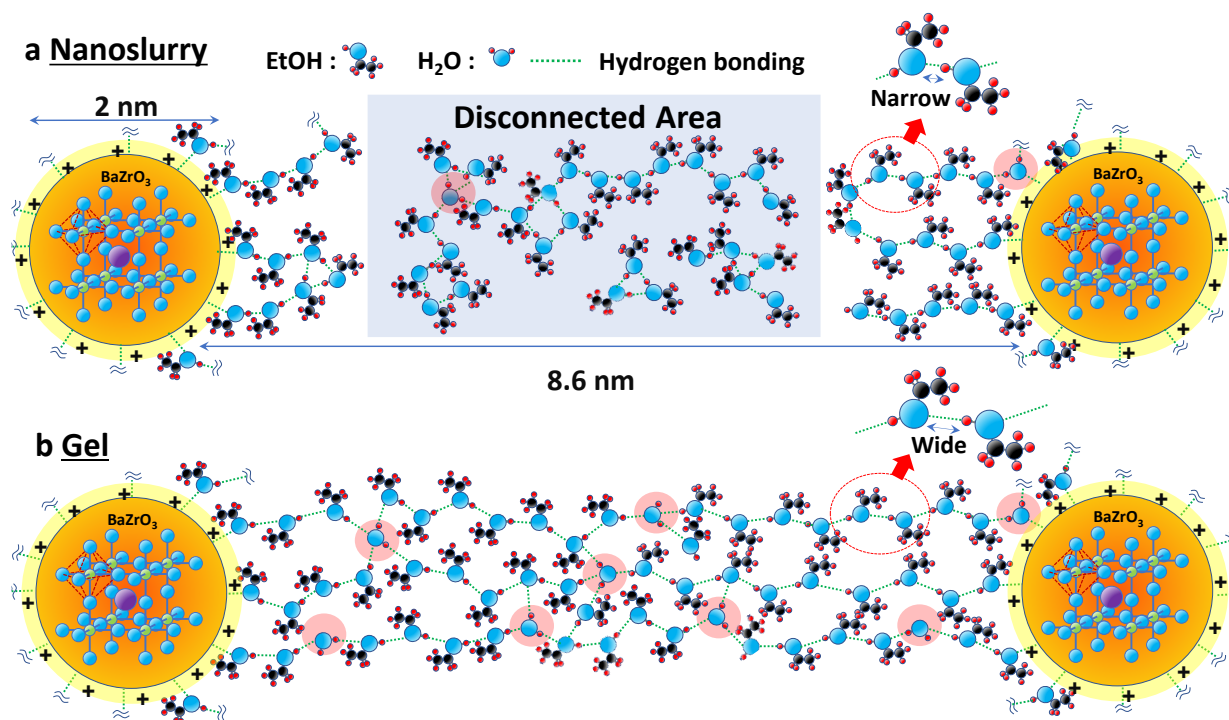All data are available in the main text or the supplementary materials.
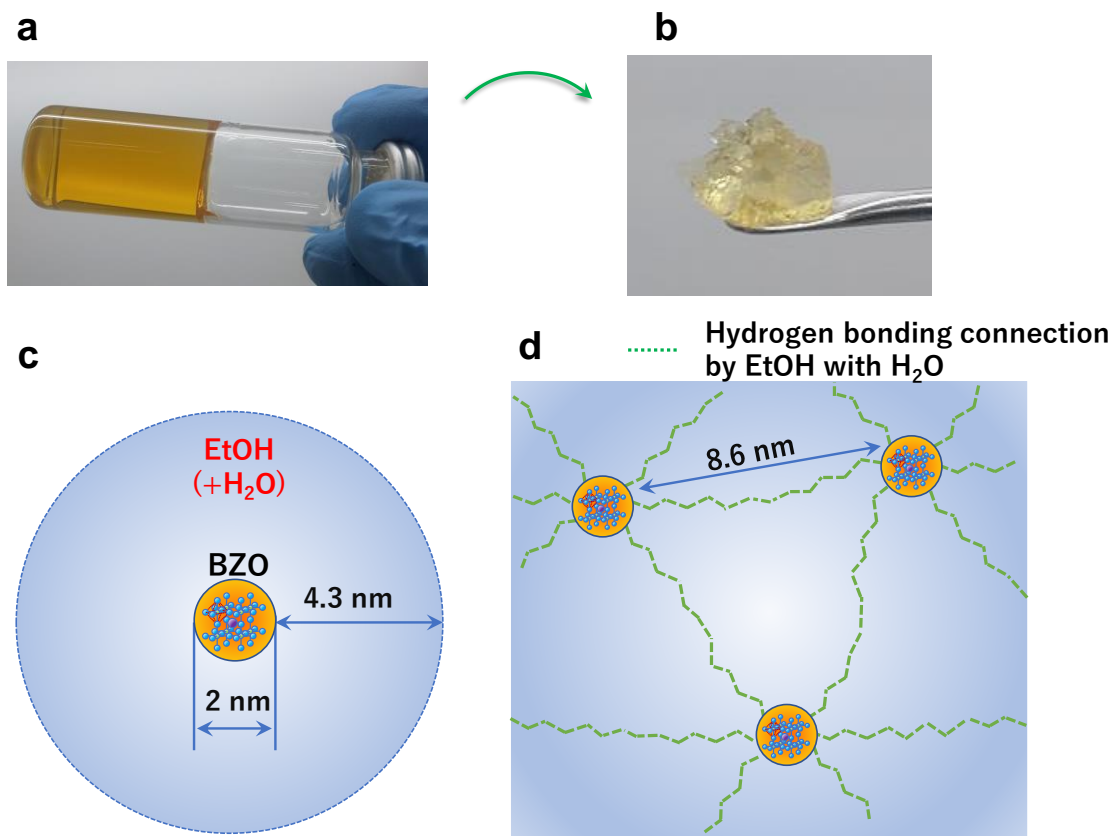
Fig. 1 | Appearance of naturally solidified BZO gel and schematic of the predicted structure of the gel (i.e., the volume ratio and distance between nanoparticles in the gel). In this case, the weight percentage of BZO in the gel is 5 wt%. a, BZO gel naturally solidified in a vial. **b,** Gel scooped with a spoon. **c,** Volume ratio estimated from BZO powder weight percentage in the gel (see the calculation in the Methods section). **d,** Expected internanoparticle distance when gelation is caused by hydrogen bonding.
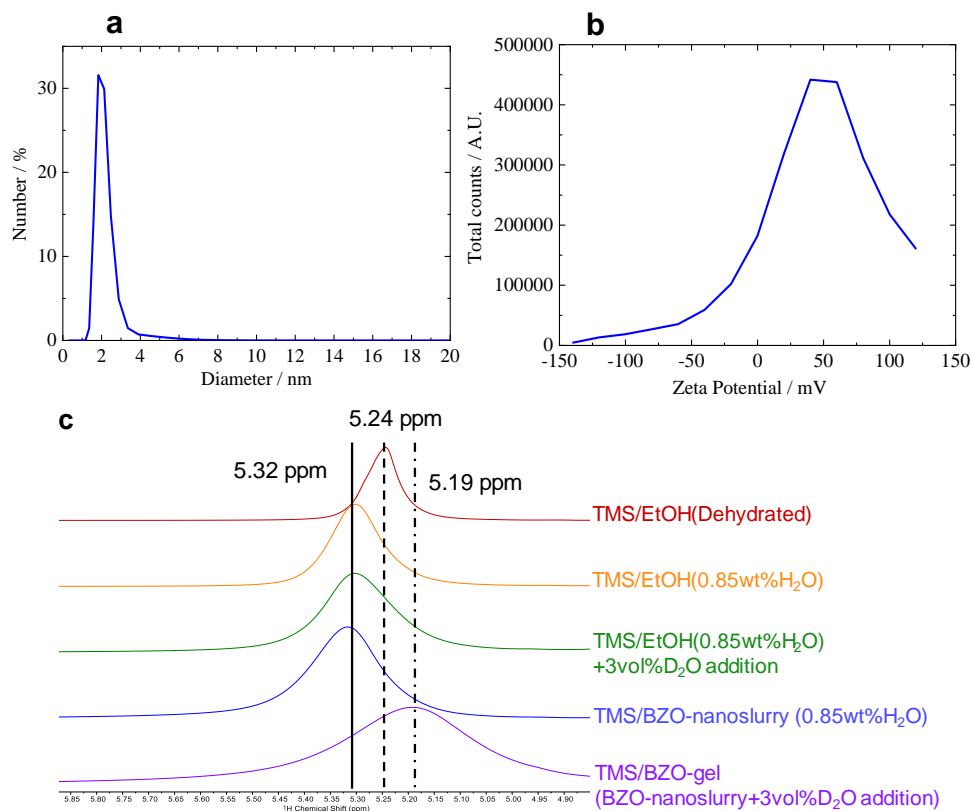
Fig. 2 | DLS–zeta potential measurements for BZO nanoparticles and ¹H-NMR spectra of the BZO nanoslurry and BZO gel. a, b, Particle size distribution and zeta potential. **c,** Comparison of the OH peak shifts in the ¹H-NMR spectra of the BZO nanoslurry, BZO gel, dehydrated EtOH, 0.85 wt% H_2O–EtOH, and 0.85 wt% H_2O–EtOH + 3 vol% D_2O addition. In this case, the water content of the BZO nanoslurry was ~0.85 wt%.
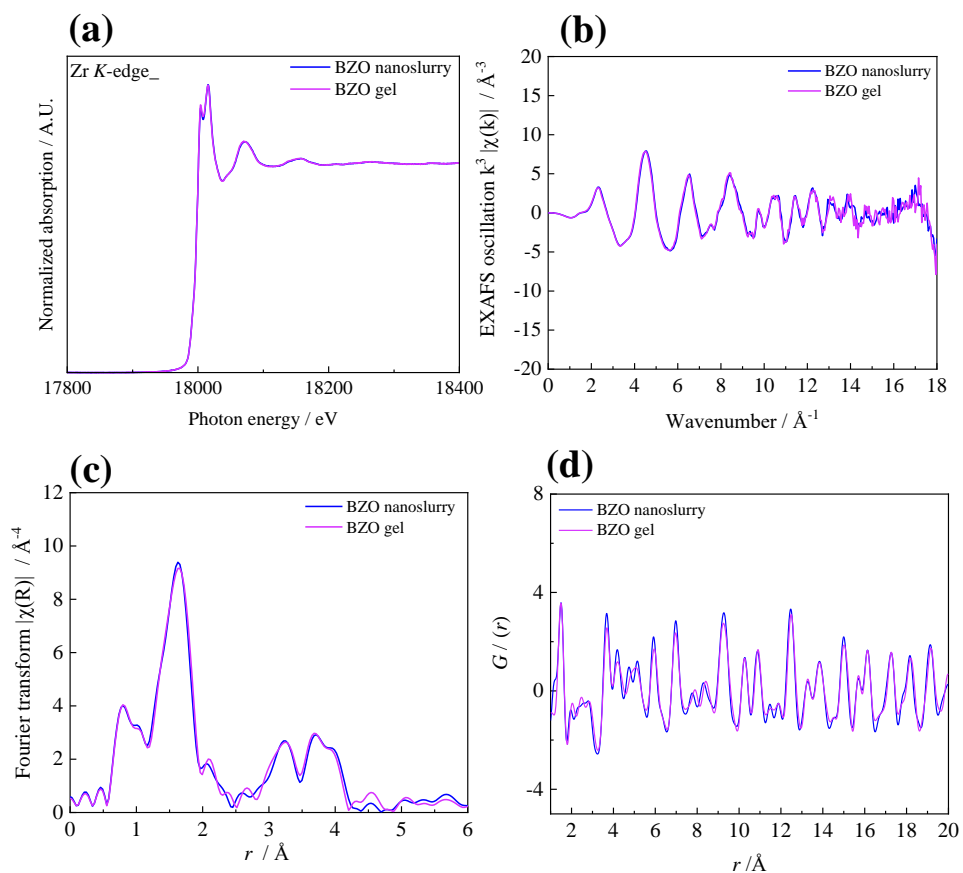
Fig. 3 | XAFS and PDF results for the BZO nanoslurry and BZO gel. a, Zr *K*-edge XANES spectra. **b,** Zr *K*-edge EXAFS oscillations. **c,** Amplitudes of the Fourier transforms obtained from EXAFS oscillations. **d,** $G(r)$ profiles.

a Nanoslurry

EtOH : H_2O :   ⋯⋯ Hydrogen bonding

2 nm

Disconnected Area

Narrow

$BaZrO_3$

$BaZrO_3$

8.6 nm

b Gel

Wide

$BaZrO_3$

$BaZrO_3$

Fig. 4 | Detailed schematic of the gel formation process for the BZO nanoslurry by hydrogen bonding. a, BZO nanoslurry (the weight percentage of BZO is 5 wt%). **b,** BZO gel (the amount of H_2O added to the slurry is 3:100 vol%).
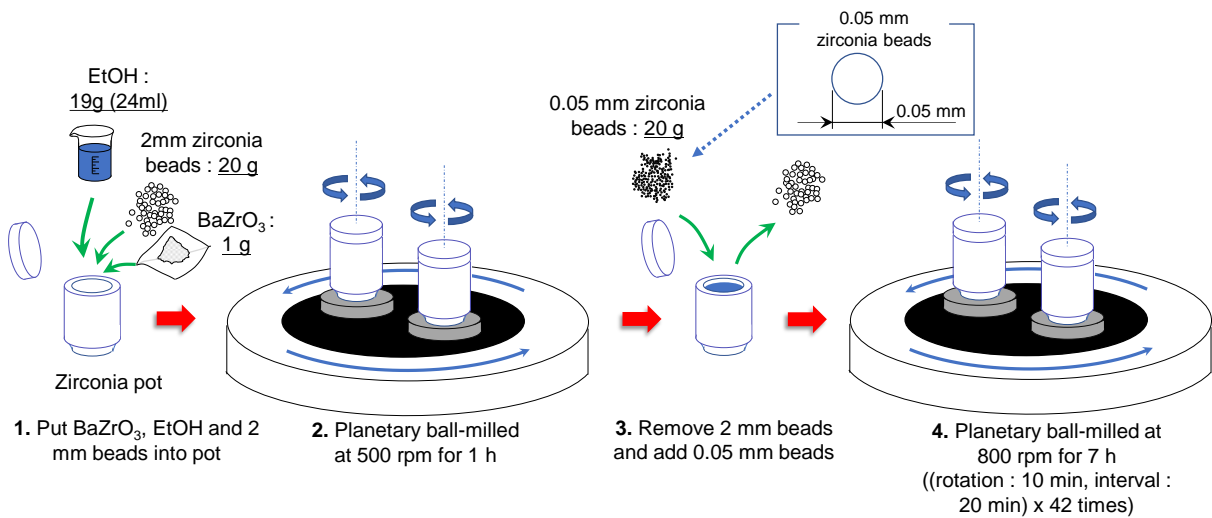
Extended Data Fig. 1 | Schematic of bead-milling procedure using zirconia beads and pots with a planetary ball-mill machine. The wt% of BZO in the nanoslurry used in this work was kept constant at ~5 wt% unless otherwise noted.

After 2 mm∅   After 0.05 mm∅
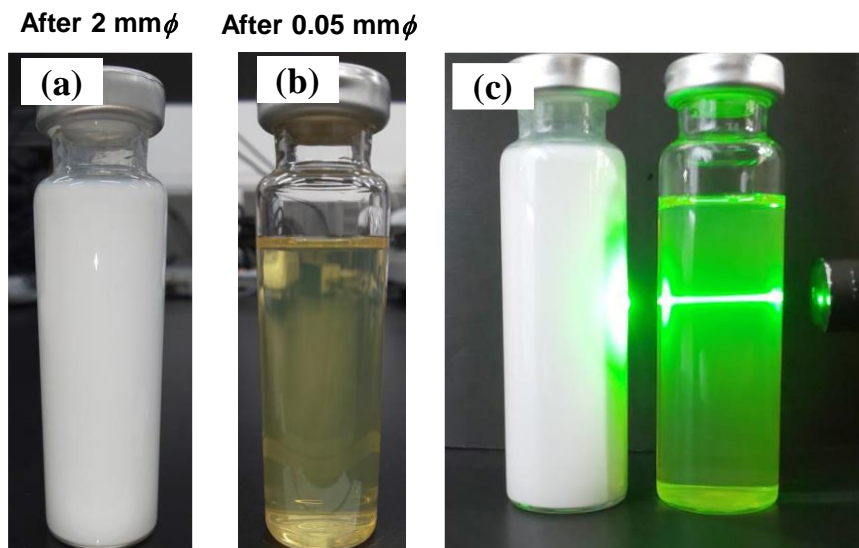
Extended Data Fig. 2 | Appearance of the bead-milling slurry before and after ⌀0.05 mm bead milling. a, Before ⌀0.05 mm bead milling (after ⌀2 mm bead milling). **b,** After ⌀0.05 mm bead milling. **c,** Slurries irradiated with laser pointer. *Note: The slurry after ⌀0.05 mm bead milling was not centrifuged. Before the ⌀0.05 mm milling, only an opaque white slurry, which precipitated immediately, was obtained (a); however, after the ⌀0.05 mm milling, the slurry became transparent (b). In addition, when the ⌀0.05 mm milling slurry was irradiated with a laser pointer, the laser penetrated the slurry and Rayleigh scattering was observed, suggesting that nanoparticles were present in the slurry (c).
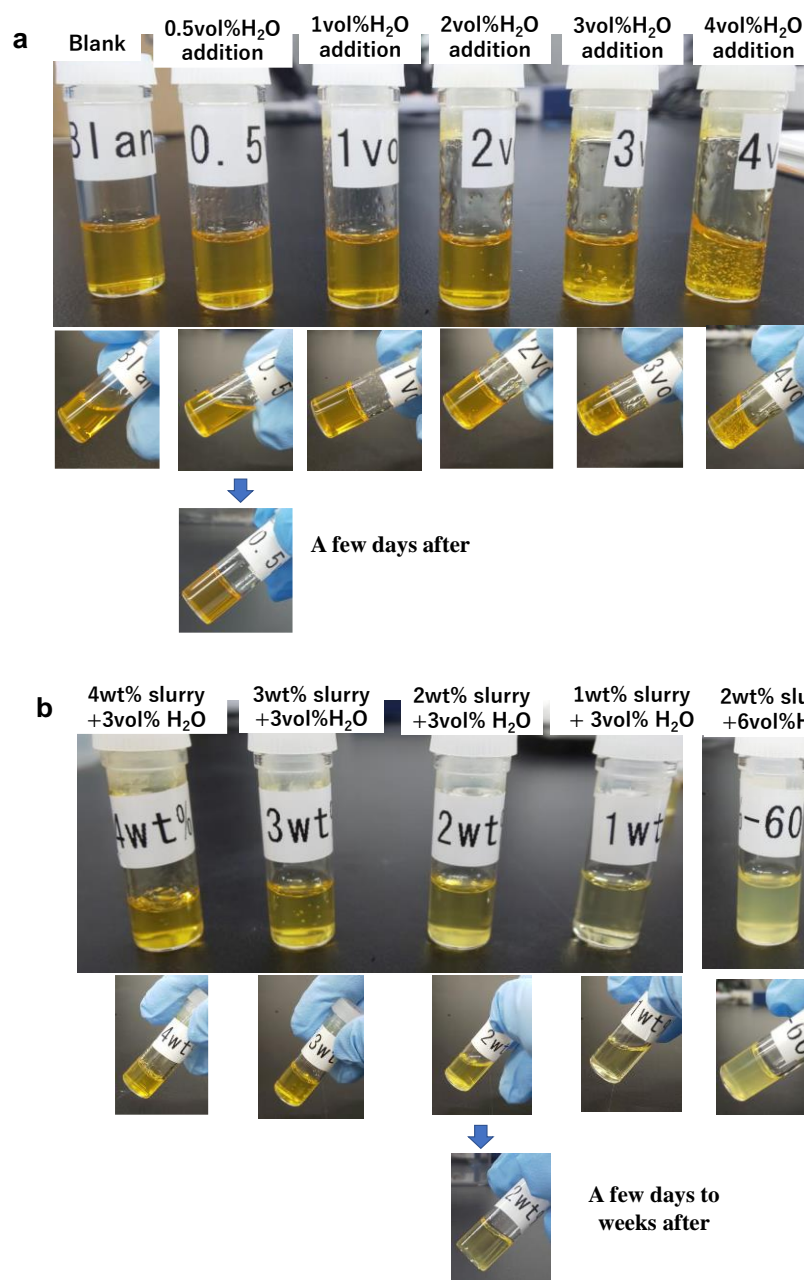
Extended Data Fig. 3 | Appearance of gelation of bead-milled slurry. a, Appearance of gelation of the bead-milled slurry when various amounts of H_2O are added. The initial H_2O content of the slurry was ~0.77 wt%. The blank (leftmost) is the sample without any H_2O added; 5, 10, 20, 30, and 40 μL H_2O were subsequently added to 1 mL of the bead-milled slurry (corresponding to 0.5, 1, 2 , 3, and 4 vol% additions, respectively). Only the 0.5 vol% H_2O-added sample took a few days to completely gelate. **b,** Appearance of gelated bead-milling slurries diluted to 4, 3, 2, and 1 wt% with dehydrated ethanol, respectively. The slurry with a H_2O content of ~0.77 wt% was used as a sample. In this case, H_2O was added to the slurries at 3:100 vol% (except the rightmost sample, where H_2O was added at 6 vol%). Gelation was observed at slurry concentrations as low as 2 wt%, although gelation required a long time. However, even at 2 wt%, gelation was accelerated when the H_2O addition was increased to 6 vol%.

Before bead milling（EtOH）: 1271 ppm

**After Bead milling（BZO nanoslurry）: 6401 ppm**

After bead mill
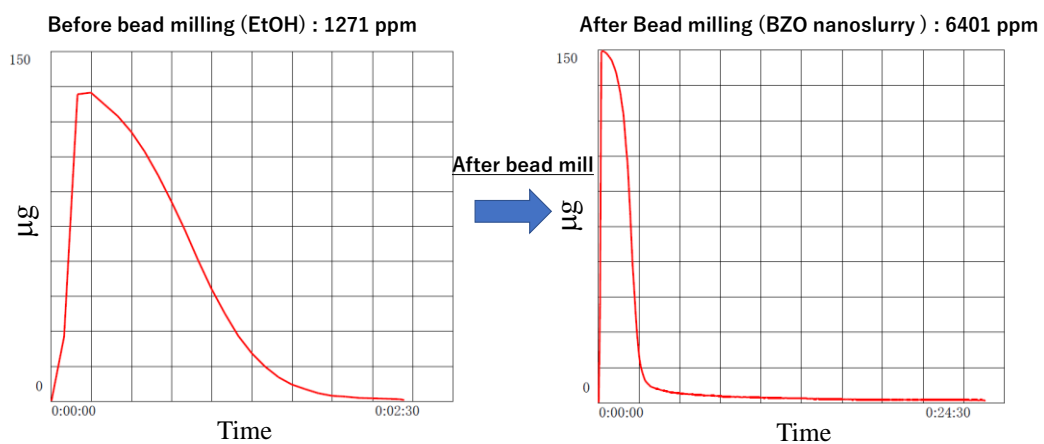
Extended Data Fig. 4 | Example of results of H₂O content analysis by Karl Fischer titration. Other results are summarized in Table S1.
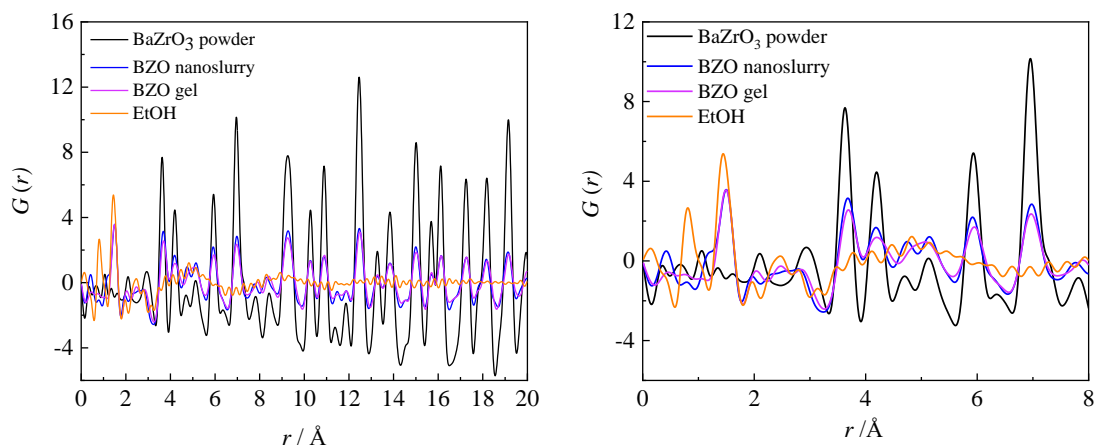
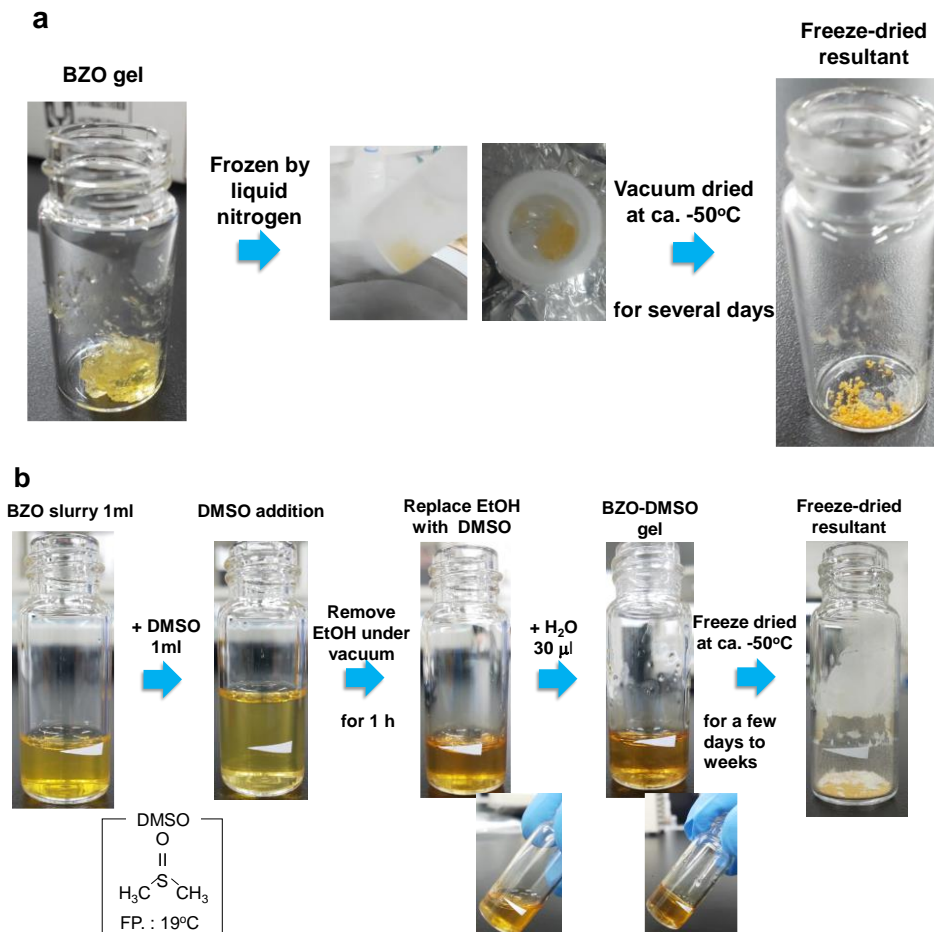**Extended Data Fig. 5 | $G(r)$ profiles for BZO nanoslurry, BZO gel, ⌀2 mm milling slurry, and BZO powder.** The BZO gel was obtained by adding H_2O to the BZO slurry at 3:100 vol%. *Note: We do not assume a structure with correlations below 1 Å; hence, the spectra below 1 Å are eliminated in Fig. 3. This result indicates that the local structure derived from the short-range correlations is slightly changed, whereas no change is observed in the medium- and long-range correlations, suggesting that the nanoparticles in the BZO nanoslurry and gel retain the same average perovskite structure as that of the BZO powder.
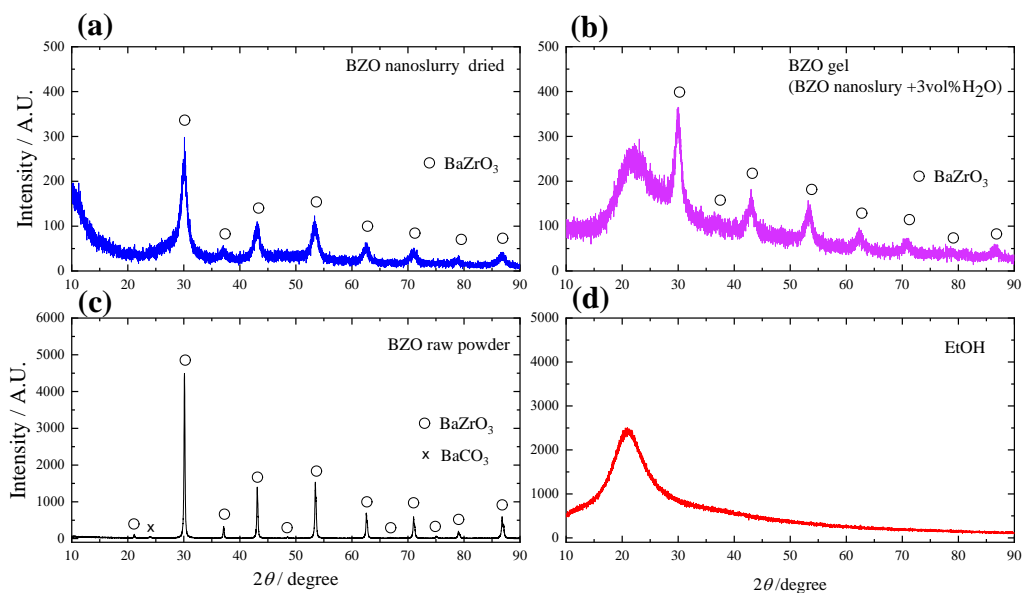
Extended Data Fig. 6 | XRD patterns for dried BZO nanoslurry, BZO gel (3 vol% H_2O addition), BZO raw powder, and ethanol. a–d, Patterns of dried BZO nanoslurry, BZO gel, BZO raw powder, and ethanol, respectively. The BZO raw powder is almost single-phase, and the diffraction peaks of BZO are confirmed in the XRD patterns for both the BZO nanoslurry and the gel. In addition, the widths of the BZO nanoslurry and gel peaks are broadened, indicating that these samples are nanosized. The broad peak observed at ~20° in the pattern of the BZO gel (b) is attributed to the scattering by ethanol, as shown in (d).
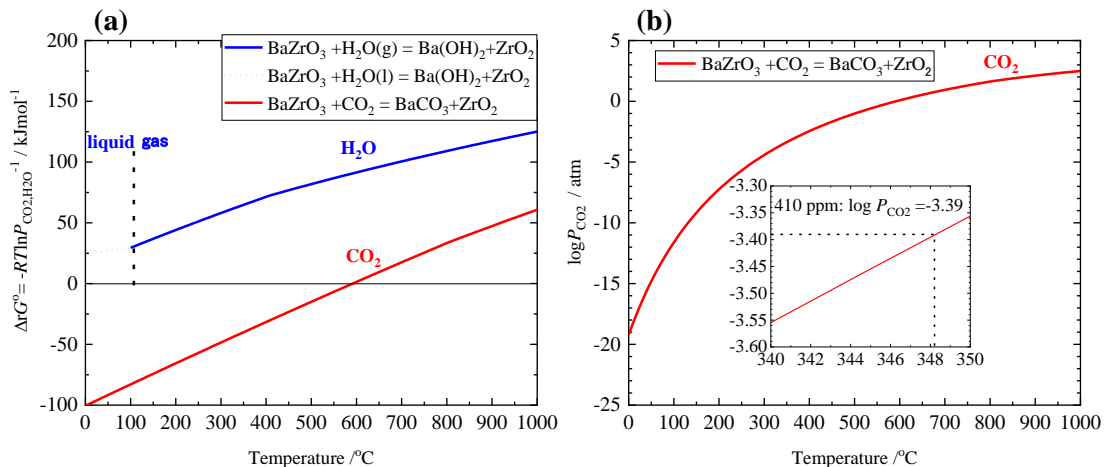
Extended Data Fig. 7 | Calculation results of the thermodynamic stability of BaZrO₃ against H₂O and CO₂ using MALT-2. a, In the case of H₂O, the stability was calculated with 1 bar gas (vapor) at temperatures greater than 100 °C and with liquid water at temperatures less than 100 °C. The calculations indicate that $BaZrO_3$ is not decomposed by H_2O over the full investigated temperature range (from 0 to 1000 °C). **b,** As is well known, BZO undergoes decomposition in the presence of 410 ppm CO_2 (the CO_2 content of ambient air) at temperatures less than 350 °C. Therefore, as mentioned in the description of the XRD analysis, the bead-milling slurry was dried in vacuum and the XRD measurements were conducted immediately thereafter.

a

BZO gel

Frozen by liquid nitrogen

Vacuum dried at ca. -50°C

for several days

Freeze-dried resultant

b

BZO slurry 1ml

DMSO addition

+ DMSO 1ml

Remove EtOH under vacuum

for 1 h

Replace EtOH with DMSO

+ H₂O 30 μl

BZO-DMSO gel

Freeze dried at ca. -50°C

for a few days to weeks

Freeze-dried resultant

DMSO
$$\underset{H_3C}{}\overset{O}{\underset{}{\overset{\|}{S}}}\underset{CH_3}{}$$
FP. : 19°C

Extended Data Fig. 8 | Appearance of BZO gel. a, Appearance of the naturally solidified BZO gel, which was frozen in liquid N_2 and freeze-dried under vacuum at approximately −50 °C for several days. The lack of a xerogel-like material was confirmed. **b,** Appearance of freeze-dried BZO slurry after replacement with dimethyl sulfoxide (DMSO), which is an organic material with a high melting point. The DMSO replacement was performed by evaporating the ethanol under vacuum after the addition of DMSO. Eventually, no xerogel-like material was observed.
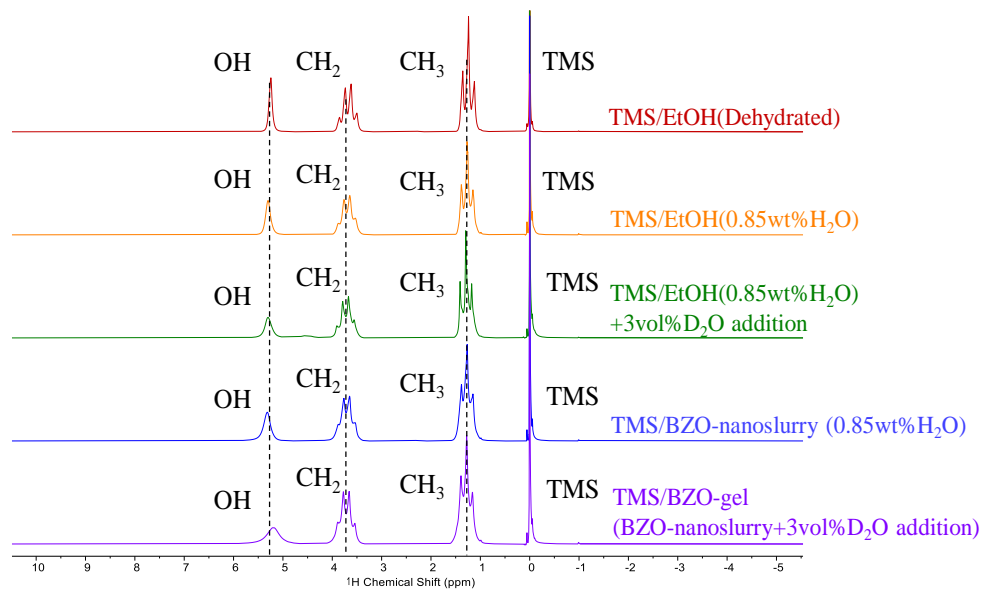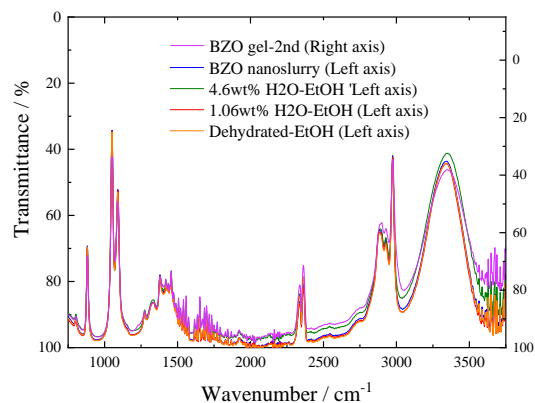
Extended Data Fig. 9 | ^{1}H-NMR spectra of BZO nanoslurry, BZO gel, dehydrated ethanol, 0.85 wt% H$_2$O–EtOH, and 3 vol% D$_2$O addition 0.85 wt% H$_2$O–EtOH. Here, the water content of the BZO nanoslurry was ~0.85 wt%.
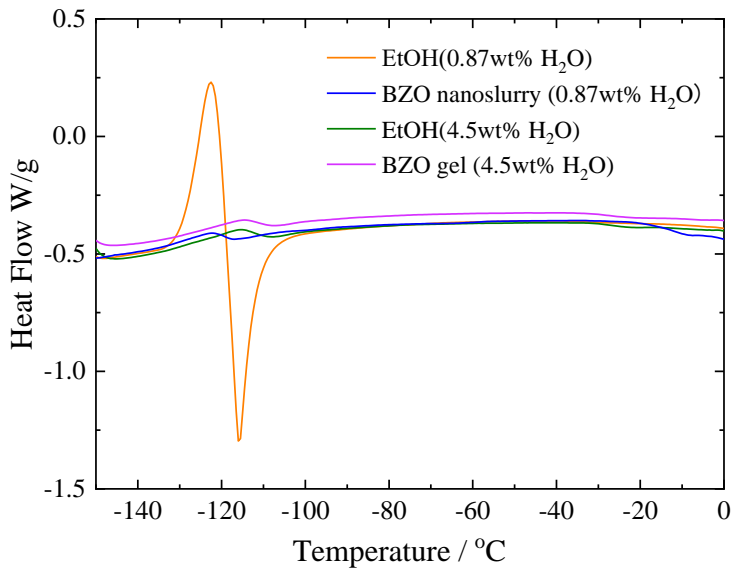
Extended Data Fig. 10 | Low-temperature DSC curves for BZO nanoslurry, BZO gel, and ethanol with H₂O added. The H_2O content of the BZO nanoslurry was ~0.87 wt%, and the BZO gel was obtained by adding 3 vol% H_2O to the 100 vol% BZO nanoslurry (its total H_2O content is 4.5 wt%). In addition, ethanol solutions with same H_2O content as these samples were also measured for comparison. Large peaks are observed in the case of 0.87 wt% H_2O–ethanol because 0.87 wt% H_2O–ethanol has a higher purity (less H_2O and fewer nanoparticles), which enables the clean crystallization of ethanol.
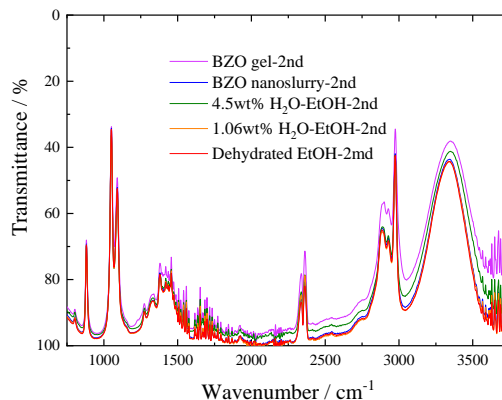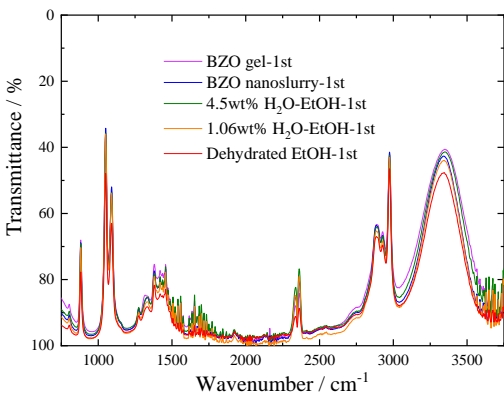
Extended Data Fig. 11 | ATR FT-IR spectra of BZO nanoslurry, BZO gel, dehydrated ethanol, 1.06 wt% H₂O–ethanol, and 4.6 wt% H₂O–ethanol. The water content of the BZO nanoslurry was 1.06 wt%, and the BZO gel was obtained by adding 3 vol% H_2O to the nanoslurry of 100 vol% (its total water content was 4.6 wt%). (a) First measurement, (b) second measurement, and (c) the spectra corresponding to the second measurement normalized by the height of the peak at 3000 cm^{-1}. In both spectra, unlike the case for ethanol bonds on the silicon surface in cyclohexane solution (Ref. 7 in the main text), no substantial change in the OH stretching vibration peak at 3000–3500 cm^{-1} was observed. That is, a substantial increase or strengthening of the hydrogen bonds of ethanol is not the reason for the gelation.

Extended Data Table 1 | Typical water content of BZO nanoslurry and ethanol used in this work. The water content was obtained by Karl Fischer titration. After the bead milling, the water content was increased to approximately 6000–10,000 ppm (0.6 to 1 wt%).

Sample No.	H_2O wt % in EtOH used for bead milling	H_2O wt % in BZO slurry after bead milling
1.	1271 ppm	7299 ppm
2.	1271 ppm	6401 ppm
3.	715 ppm	10602 ppm
4.	715 ppm	8815 ppm
5.	704 ppm	7580 ppm
6.	704 ppm	8587 ppm
7.	888 ppm	7716 ppm
8.	888 ppm	8853 ppm
9.	1034 ppm	7318 ppm
10.	1034 ppm	8730 ppm
11.	730 ppm	7710 ppm
12.	730 ppm	8579 ppm
13.	529 ppm	8451 ppm
14.	529 ppm	10562 ppm

Extended Data Table 2 | Peak-top temperature values derived from the low-temperature DSC curves for the respective samples. The peak-top temperature 1 and peak-top temperature 2 correspond to the crystallization temperature and melting temperature for ethanol, respectively. For both the BZO nanoslurry and gel, these temperatures are approximately the same as those for ethanol with the same water content, suggesting that the condition of ethanol in the BZO slurry and gel is similar to that of ethanol with the same water content.

	Peak top temperature 1/ °C	Peak top temperature 2/ °C
EtOH(0.87wt%H_2O)	-122.57	-115.79
BZO nanoslurry (0.87wt%H_2O)	-122.25	-117.16
EtOH (4.5wt%H_2O)	-115.41	-108.06
BZO gel (4.5wt%H_2O)	-114.47	-107.21